

Serveur Académique Lausannois SERVAL [serval.unil.ch](http://serval.unil.ch)

## Author Manuscript

Faculty of Biology and Medicine Publication

This paper has been peer-reviewed but does not include the final publisher proof-corrections or journal pagination.

Published in final edited form as:

**Title:** Functional assessment of sodium chloride cotransporter NCC mutants in polarized mammalian epithelial cells.

**Authors:** Rosenbaek LL, Rizzo F, MacAulay N, Staub O, Fenton RA

**Journal:** American journal of physiology. Renal physiology

**Year:** 2017 Aug 1

**Issue:** 313

**Volume:** 2

**Pages:** F495-F504

**DOI:** 10.1152/ajprenal.00088.2017

In the absence of a copyright statement, users should assume that standard copyright protection applies, unless the article contains an explicit statement to the contrary. In case of doubt, contact the journal publisher to verify the copyright status of an article.

1 **Functional Assessment of Sodium Chloride Co-transporter NCC Mutants**  
2 **in Polarized Mammalian Epithelial Cells**

3  
4 Lena L Rosenbaek<sup>1,2</sup>, Federica Rizzo<sup>3,4</sup>, Nanna MacAulay<sup>2</sup>, Olivier Staub<sup>3,4</sup> and Robert A.  
5 Fenton<sup>1</sup>

6  
7 *<sup>1</sup>InterPrET Center, Department of Biomedicine, Aarhus University, Aarhus DK-8000,*  
8 *Denmark, <sup>2</sup>Department of Neuroscience and Pharmacology, University of Copenhagen,*  
9 *Copenhagen, Denmark, <sup>3</sup>Department of Pharmacology & Toxicology, University of*  
10 *Lausanne, Lausanne, Switzerland, <sup>4</sup>National Centre of Competence in Research*  
11 *“Kidney.ch”, Switzerland*

12  
13  
14  
15 **Running title:** NCC uptake assay in polarized mammalian cells

16  
17  
18 **Keywords:** *Slc12a3*, thiazide-sensitive co-transporter, cotransporter, phosphorylation,  
19 sodium flux assay

20  
21  
22 **Correspondence:**

23 Robert A. Fenton  
24 Aarhus University  
25 Institute for Biomedicine  
26 Wilhelm Meyers Allé 3, Building. 1233  
27 DK- 8000 Aarhus C  
28 Denmark  
29 Tel: +0045 87167671  
30 E-mail: [robert.a.fenton@biomed.au.dk](mailto:robert.a.fenton@biomed.au.dk)

31

32 **Abstract**

33

34 The thiazide-sensitive sodium chloride cotransporter, NCC, is important for maintaining  
35 serum sodium ( $\text{Na}^+$ ) and, indirectly, serum potassium ( $\text{K}^+$ ) levels. Functional studies on NCC  
36 have used cell lines with native NCC expression, transiently transfected non-polarized cell  
37 lines or *Xenopus laevis* oocytes. Here, we developed the use of polarized Madin-Darby  
38 canine kidney type I (MDCKI) mammalian epithelial cell lines with tetracycline-inducible  
39 human NCC expression to study NCC activity and membrane abundance in the same  
40 system. In radiotracer assays, induced cells grown on filters had robust thiazide-sensitive  
41 and chloride dependent sodium-22 ( $^{22}\text{Na}$ ) uptake from the apical side. To minimize cost and  
42 maximize throughput, assays were modified to use cells grown on plastic. On plastic, cells  
43 had similar thiazide-sensitive  $^{22}\text{Na}$  uptakes that increased following pre-incubation of cells  
44 in chloride-free solutions. NCC was detected in the plasma membrane and both membrane  
45 abundance and phosphorylation of NCC were increased by incubation in chloride-free  
46 solutions. Furthermore, in cells exposed for 15 min to low or high extracellular  $\text{K}^+$ , the levels  
47 of phosphorylated NCC increased and decreased, respectively. To demonstrate that the  
48 system allows rapid and systematic assessment of mutated NCC, three phosphorylation  
49 sites in NCC were mutated and NCC activity examined.  $^{22}\text{Na}$  fluxes in phosphorylation  
50 deficient mutants were reduced to baseline levels, whereas phosphorylation mimicking  
51 mutants were constitutively active – even without chloride-free stimulation. In conclusion,  
52 this system allows the activity, cellular localization, and abundance of wildtype or mutant  
53 NCC to be examined in the same polarized mammalian expression system in a rapid, easy,  
54 and low cost fashion.

55

56

57 **Introduction**

58  
59           The kidney plays a key role in blood pressure control by modulating the levels of NaCl  
60 reabsorption. Although the majority of NaCl reabsorption occurs in the proximal tubules, the  
61 distal convoluted tubules (DCT) play an essential role in the fine-tuning of tubular fluid NaCl  
62 concentrations. DCT NaCl transport is tightly regulated by a variety of hormones e.g.  
63 vasopressin (8, 29) and angiotensin II (35, 42), which exert the majority of their effects by  
64 modulating the function of the sodium chloride cotransporter NCC, the predominant NaCl  
65 entry pathway in this segment (reviewed in (10)). NCC is a member of the SLC12  
66 electroneutral cation-coupled chloride cotransporter family, which also includes the sodium  
67 potassium chloride cotransporters, NKCC1 and NKCC2, as well as several potassium  
68 chloride cotransporters (KCCs). Inactivating mutations of NCC lead to the autosomal  
69 recessive kidney disorder Gitelman syndrome, characterized by hypokalemia,  
70 hypomagnesemia, metabolic alkalosis, and hypocalciuria (22, 24, 27, 36). In Gordon's  
71 syndrome (PHAII or familial hyperkalemic hypertension), increased activity of NCC is  
72 observed, resulting in hyperkalemic hypertension (15).

73           In the last few years, a large number of studies performed using *Xenopus laevis*  
74 oocytes (14, 28, 34, 43) or mammalian cell lines expressing native NCC (5, 13, 19-21, 32),  
75 have advanced our understanding on how alterations in NCC localization or NCC activity  
76 interplay to determine the final rate of NaCl reabsorption (reviewed in (26)). For example, 1)  
77 the activity of NCC is regulated by posttranslational modifications such as phosphorylation,  
78 ubiquitylation, and glycosylation (11, 17); 2) NCC is functional in a highly glycosylated  
79 homodimeric form (6, 12, 17, 31); 3) phosphorylation of NCC is critical for maximal NaCl  
80 transport capacity (15) and can alter NCC membrane abundance (33); 4) phosphorylation  
81 of NCC is regulated by a variety of hormonal stimuli, which exert several of their effects via

82 activation of the WNK-SPAK kinase cascade (15) Despite these major advances, a limitation  
83 in the field has been the lack of a suitable system that allows a direct comparison of NCC  
84 activity and localization in a polarized mammalian cell system alongside the capacity to  
85 examine wildtype NCC or various forms of NCC carrying targeted mutations e.g. specific  
86 post-translational modification or Gitelman's causing mutations. Therefore, the aim of this  
87 study was to develop a  $^{22}\text{Na}$  uptake assay for direct assessment of the function of wildtype  
88 or mutant NCC in a polarized mammalian cell line. The assays are based on Type I MDCK  
89 (Madin-Darby Canine Kidney) cells containing FRT (flippase recognition target) sites with  
90 tetracycline-inducible NCC expression (33). We demonstrate that these cells can be rapidly  
91 modified to express various forms of NCC from a single genomic site, allowing direct  
92 comparison of the abundance, activity, and localization of wildtype and mutant NCC in a  
93 single system.

94

95

96 **Materials and Methods**

97 *Antibodies* – The antibodies used in this study are rabbit polyclonal antibodies against total  
98 NCC (a kind gift from Dr. Mark Knepper, NIH, Bethesda, Maryland, USA)(18),  
99 phosphorylated NCC (pT58) (29) and FLAG-tag (F7425, Sigma).

100

101 *Generation of tetracycline inducible NCC expressing MDCKI cell lines* - A FLAG-tag  
102 (GACTACAAGGACGATGACGATAAG; amino acids DYKDDDDK) was introduced into the  
103 NH<sub>2</sub>-terminus of a human NCC (hNCC) cDNA using standard methods. Using PCR, the  
104 FLAG-tagged hNCC sequence was subcloned into the pcDNA5/FRT/TO/TOPO vector  
105 (Invitrogen). The pcDNA5/FRT/TO/TOPO-hNCC plasmid was cotransfected with pOG44  
106 (encoding flp recombinase) into tetracycline inducible MDCK type I cells line containing a  
107 single FRT site in their genome (33) using Lipofectamine 2000 (Invitrogen). Cells with stable  
108 insertion of the hNCC into the FRT site were selected using 500 µg/ml Hygromycin B. Stable  
109 MDCKI-hNCC cell lines were maintained in DMEM High Glucose with 10% DBS, 150 µg/ml  
110 Hygromycin B, and 5 µg/ml Blasticidin HCl. Generation of the various MDCKI-rNCC cell  
111 lines have been described previously (33).

112

113 *Quantitative reverse transcriptase PCR (RT-qPCR) and standard RT-PCR* - RNA was  
114 purified using the RiboPure™ kit (Ambion) following the manufacturer's protocol. Potential  
115 DNA contamination was removed by incubating RNA (500ng) with DNase I Amp Grade 1 in  
116 DNase Reaction buffer (20 mM Tris-HCl, pH 8.4, 2 mM MgCl<sub>2</sub>, 50 mM KCl) (Invitrogen) for  
117 15 min at room temperature. 1.1 mM EDTA was added, and the samples were heated to 65  
118 °C for 10 min to stop the DNase reaction. cDNA was produced following the protocol from  
119 SuperScript™ II reverse transcriptase (Invitrogen). Subsequently, 250 ng cDNA and 10

120 pmole gene specific primer were used for qPCR using LightCycler® 480 SYBR Green I  
 121 Master (Roche). The reaction was carried out by a LightCycler® 480 (Roche) using NCC  
 122 specific primers (forward: 5'TCCTCAAGCAGGAAGGTAGC3', reverse:  
 123 5'GTTCTCCAGGGCTCTTCTCG3'). Primers against 18SrRNA were used for normalization  
 124 (forward: 5'GGATCCATTGGAGGGCAAGT3', reverse:  
 125 5'ACGAGCTTTTAACTGCAGCAA3'). For standard RT-PCR, cDNA was generated in a  
 126 similar manner from MDCK cells or dog kidney RNA (Zyagen) and PCR performed using  
 127 HotStarTaq (Qiagen), 250 ng cDNA and 10 pmole gene specific primers and standard  
 128 conditions. Primers used were: *Slc12a2* (forward: 5'-GCCCTGCTGTCCCCTTAAAT,  
 129 reverse: 5'-CGTGCAACTGGGAGACTCAT), *Slc12a1* (forward: 5'-  
 130 GCTGAACATCTGGGGTGTCA-, reverse: 5'-CCTTTTGTGAAGCTTGGCCC), *Slc26a4*  
 131 (forward: 5'-CGATCCATAGCCTCGTGCTT, reverse: 5'-CCGGTGGGTAAATCTTGCCT),  
 132 *Slc4a8* (forward: 5'-GACTACCGGGATGCACTCAG-, reverse: 5'-  
 133 ATTGGCCCACTGGACTTCTG), *Scnn1a* (forward: 5'-CGAAGTCCCTGTGGAGAACC,  
 134 reverse: 5'-CTCCGCATTCTTGGGCAATG ), *Slc9a1* (forward: 5'-  
 135 CGAGGACATCTGTGGCCATT, reverse: 5'-GATAACAGGCAAGTCGGCCT), *Slc9a3*  
 136 (forward: 5'-GCGAACATCACTCAAGACGC, reverse: 5'-GATCCTGACATCTCAGCGGG),  
 137 *Kcnj10* (forward: 5'-CCTCTTCTCCCTCGAATCGC, reverse: 5'-  
 138 TGTCGACCTGGAAAGTCACG).

139

140 *Sample preparation and immunoblotting* – Cells were washed in PBS-CM (PBS, 1 mM  
 141 CaCl<sub>2</sub>, 0.1 mM MgCl<sub>2</sub>, pH 7.5), solubilized in 1x Laemmli sample buffer (62.5 mM Tris base  
 142 pH 6.8, 8.7% glycerol, 2% SDS, 1% bromphenolblue, 100 mM dithiothreitol) and heated for  
 143 15 min at 60 °C. SDS-PAGE was performed on 4-15% gradient polyacrylamide gels

144 (Criterion TGX Precast Protein Gels, BioRad) and transferred to PVDF membrane.  
145 Antibody-antigen reactions were visualized using SuperSignal West Femto  
146 chemiluminescent substrate (Thermo Scientific, Denmark). Semi-quantitative data were  
147 obtained by analysis of band densities using Image Studio Lite (Qiagen) and relative  
148 abundance ratios for each individual sample for each time point or stimulant were calculated.  
149 All reported values are means  $\pm$  S.E.M.

150

151 *Cell surface biotinylation assay* - Cells were grown in complete DMEM (DMEM High  
152 Glucose, 10% DBS) to confluency. Cells were induced with 10  $\mu$ g/ml tetracycline for 16-20  
153 hours prior to biotinylation. Cells were washed twice in isotonic buffer (135 mM NaCl, 5 mM  
154 KCl, 1 mM CaCl<sub>2</sub>, 1 mM MgCl<sub>2</sub>, 1 mM Na<sub>2</sub>HPO<sub>4</sub>, 1 mM Na<sub>2</sub>SO<sub>4</sub>, 15 mM Na<sup>+</sup> HEPES, pH  
155 7.4) and stimulated with either low chloride buffer (67.5 mM Na<sup>+</sup> gluconate, 2.5 mM K<sup>+</sup>  
156 gluconate, 0.5 mM CaCl<sub>2</sub>, 0.5 mM MgCl<sub>2</sub>, 1 mM Na<sub>2</sub>HPO<sub>4</sub>, 1 mM Na<sub>2</sub>SO<sub>4</sub>, 7.5 mM Na<sup>+</sup>  
157 HEPES, pH 7.4) or isotonic buffer and incubated for 20 min at 37 °C. Cells were washed in  
158 ice-cold PBS-CM and incubated with mild agitation for 30 min at 4 °C in ice-cold biotinylation  
159 buffer (10 mM triethanolamine, 2 mM CaCl<sub>2</sub>, 125 mM NaCl, pH 8.9) containing a 1 mg/ml  
160 final concentration of sulfosuccinimidyl 2-(biotin-amido)-ethyl-1,3-dithiopropionate (EZ-link  
161 Sulfo-NHS-SS-biotin, Pierce). Cells were washed in ice-cold quenching buffer (PBS-CM, 50  
162 mM Tris-HCl, pH 8) followed by two washes of PBS-CM. Cells were lysed and biotinylated  
163 proteins purified using NeutrAvidin gel slurry (Pierce) as previously described (33).

164

165 *Immunoprecipitation (IP)* - Performed as previously described (33).

166

167 *Extracellular K<sup>+</sup> manipulation* - Cells were grown in complete DMEM (DMEM High Glucose,  
168 10% DBS) to confluency and induced with 10 µg/ml tetracycline for 16-20 hours prior to  
169 experiment. Cells were washed twice in Ringer solution (98.5 mM NaCl, 3 mM KCl, 2.5 mM  
170 CaCl<sub>2</sub>, 1.8 mM MgCl<sub>2</sub>, 1 mM NaH<sub>2</sub>PO<sub>4</sub>, 25 mM NaHCO<sub>3</sub>, 25 mM glucose) and incubated for  
171 15 min at 37 °C in either Ringer solution, Ringer solution containing 1mM KCl, Ringer  
172 solution containing 6mM KCl, or low chloride buffer. An equimolar adjustment of NaCl  
173 ensured that osmolality of the solutions remained constant between the different [K<sup>+</sup>]  
174 (100.5mM NaCl or 95.5 mM NaCl). Cells were solubilized in 1x Laemmli sample buffer.

175

176 *<sup>22</sup>Na uptake assay to measure NCC activity* - Cells were grown in complete DMEM to  
177 confluency and induced for 16-20 hours with 10 µg/ml tetracycline. Subsequently, cells were  
178 washed in pre-heated (37°C) serum free DMEM medium and incubated (where indicated)  
179 for 20 min at 37°C in chloride-free buffer (130 mM Na gluconate, 2 mM K gluconate, 1 mM  
180 Ca gluconate, 1 mM Mg gluconate, 5 mM HEPES, and 5 mM Tris-HCl, pH 7.4) including 1  
181 mM Ouabain, 1 mM amiloride, 0.1 mM benzamil, and 0.1 mM bumetanide, with 0.1 mM  
182 Metolazone (where indicated). Metolazone dose response experiments were performed with  
183 concentrations ranging from 10<sup>-3</sup> to 10<sup>-8</sup> M. Cells were subsequently incubated in uptake  
184 buffer (140 mM NaCl, 1 mM CaCl<sub>2</sub>, 1 mM MgCl<sub>2</sub>, 5 mM HEPES, and 5 mM Tris pH 7.4  
185 including inhibitors) with 1.5 µCi/ml <sup>22</sup>NaCl for 20 min at 37°C. For the chloride dependency  
186 experiment, uptake was performed in either normal uptake buffer or a chloride free uptake  
187 buffer (140 mM Na gluconate, 2 mM K gluconate, 1 mM Ca gluconate, 1 mM Mg gluconate,  
188 5 mM HEPES, and 5 mM Tris-HCl, pH 7.4). Cells were rapidly and extensively washed in  
189 ice cold uptake buffer without radioisotope and lysed in 500 µl of PBS with 0.1% SDS. The  
190 average counts in the last wash from 3 samples was collected to determine background

191 activity, which was subsequently subtracted from all cell-specific radioactive measurements.  
192 All radioactivity measurements were performed in a Cobra II 5002 Auto-Gamma counter  
193 (Packard) with a counting efficiency of approximately 95%. 20 µl of each lysed sample was  
194 used to determine total protein concentration using the BCA Protein Assay Kit (Pierce).

195

196 *Statistical analysis* - One-way analyses of variance or Tukey's multiple comparisons tests  
197 were performed as appropriate using Graphpad Prism. Experimental numbers (n) are  
198 reported in individual figures. Values are considered statistically significant when  $p < 0.05$ .

199

200

201 **Results**

202 *Generation and characterization of an MDCKI cell line with tetracycline inducible human*  
203 *NCC expression.*

204 A schematic overview of the procedure for generating MDCK type I stable cell lines  
205 expressing tetracycline inducible human NCC (or another gene of interest (GOI)) is shown  
206 in Fig 1A. Several cell lines were generated and characterized based on cell morphology,  
207 NCC expression levels, and NCC trafficking to the apical plasma membrane. One individual  
208 clone (termed MDCKI-hNCC) was used for the remainder of this study. Immunoprecipitation  
209 of hNCC using a FLAG-tag antibody followed by western blotting against NCC identified  
210 hNCC as a non-glycosylated band of approximately 100 kDa, a mature glycosylated  
211 smeared band ~130 kDa, and as dimeric forms above 250 kDa (**Fig 1B**). No hNCC was  
212 detected in similar cells in the absence of tetracycline. To assess if the expression of hNCC  
213 correlated with increased NaCl transport into MDCKI cells, <sup>22</sup>Na uptake assays were  
214 developed. In MDCKI-hNCC cells grown on semi-permeable supports there was a  
215 significantly higher <sup>22</sup>Na uptake following treatment with tetracycline relative to non-treated  
216 controls (**Fig 1C**). Following incubation of tetracycline treated MDCKI-hNCC cells with  
217 metolazone (a thiazide that inhibits NCC activity), <sup>22</sup>Na uptake was decreased. A small  
218 decrease in <sup>22</sup>Na uptake was also observed in non-induced MDCKI-hNCC cells with  
219 metolazone, indicating either a small leakiness in NCC expression, or the presence of a  
220 minor alternative metolazone-sensitive NaCl entry pathway in MDCKI cells. To examine the  
221 latter possibility, the expression of other Na<sup>+</sup> transport proteins in our MDCKI-hNCC cells  
222 was examined by RT-PCR (**Fig 2**). The sodium potassium chloride cotransporter 1  
223 (NKCC1), the Na<sup>+</sup>-driven Cl<sup>-</sup>/HCO<sub>3</sub><sup>-</sup> exchanger (NDCBE), the alpha-subunit of the epithelial  
224 sodium channel (ENaC) and the sodium hydrogen exchanger 1 (NHE1) were detected in

225 our MDCKI cells, whereas NKCC2, Pendrin and the sodium hydrogen exchanger 3 (NHE3)  
226 were absent. As NDCBE is inhibited by thiazide (23, 37), it is a good candidate for the minor  
227 alternative metolazone-sensitive NaCl entry pathway in MDCKI-hNCC cells.

228

229 *Comparison of MDCKI-hNCC cells grown on plastic or semi-permeable supports.*

230 Due to the high cost of growing cells in large numbers on semi-permeable supports, and the  
231 technical difficulty in handling numerous separate filters rapidly at the same time, we wanted  
232 to transfer the uptake assay to cells grown on plastic support. Visually, MDCKI-hNCC cells  
233 grown on plastic plates formed a tight confluent monolayer of hexagonal shaped cells (**Fig**  
234 **3A**). Immunoprecipitation of hNCC using a FLAG-tag antibody from cells grown on plastic  
235 support followed by western blotting identified hNCC as a non-glycosylated band of around  
236 100 kDa and a smear of approximately 130 kDa (**Fig 3B**), corresponding to the immature  
237 non-glycosylated and mature glycosylated monomeric form of NCC, respectively. The  
238 dimeric form of NCC was not consistently observed in MDCKI-hNCC cells grown on plastic  
239 plates. No NCC was detected in non-induced cells. As previously observed (**Fig 1**),  
240 tetracycline-induced MDCKI-hNCC cells grown on semi-permeable supports had a  
241 significantly higher metolazone sensitive  $^{22}\text{Na}$  uptake relative to non-treated controls (**Fig**  
242 **3C**). Metolazone sensitive  $^{22}\text{Na}$  uptake was also observed in MDCKI-hNCC cells grown on  
243 plastic. However, the magnitude of  $^{22}\text{Na}$  uptake in plastic grown cells relative to semi-  
244 permeable supports was significantly less (**Fig 3C**). The reduced uptake in plastic grown  
245 cells relative to semi-permeable support grown cells corresponded with significantly less  
246 hNCC (**Fig. 3D and E**). As metolazone sensitive  $^{22}\text{Na}$  uptake could consistently be  
247 measured in MDCKI-hNCC cells grown on plastic, the remainder of studies were performed  
248 on this support.

249

250 *Characterization of  $^{22}\text{Na}$  uptake in MDCKI-hNCC cells grown on plastic supports*

251 To further assess the characteristics of  $^{22}\text{Na}$  uptake in plastic grown MDCKI-hNCC cells, the  
252 effects of uptake time, metolazone dose, and chloride dependency were determined.  
253 Incubation of tetracycline-induced cells in uptake solution for various times demonstrated  
254 increased  $^{22}\text{Na}$  uptake as a function of time, with apparent time-linearity up to 40 min ( $r^2 =$   
255 0.95, no significant deviation from linearity) (**Fig 4A**). To ensure all uptakes were performed  
256 within the linear range, we continued to perform subsequent uptakes with a 20 min  
257 incubation time. Metolazone inhibition experiments allowed generation of a dose-response  
258 curve of  $^{22}\text{Na}$  uptake (**Fig. 4B**). The calculated  $\text{IC}_{50}$  for metolazone was  $0.43 \times 10^{-6}\text{M}$ , with  
259 maximal inhibition of  $^{22}\text{Na}$  uptake occurring between 3-10  $\mu\text{M}$ . The degree of  $^{22}\text{Na}$  uptake in  
260 MDCKI-hNCC cells incubated in uptake medium without chloride ions (chloride-free buffer,  
261 CF) was comparable to levels after metolazone inhibition, demonstrating chloride  
262 dependency of the  $^{22}\text{Na}$  uptake and indicating a requirement for NCC in the transport  
263 process (**Fig. 4C**).

264

265 *Chloride-free pre-incubation of MDCKI-hNCC cells increases  $\text{Na}^+$  uptake*

266 We have previously shown that incubation of semi-permeable support grown MDCKI cells  
267 expressing rat NCC in low chloride medium increases apical plasma membrane abundance  
268 of NCC and phosphorylation of NCC at an activating site (pT58-NCC). These events are  
269 associated with decreased rates of NCC internalization (33). Similar results are observed  
270 for plastic grown MDCKI-hNCC cells, with the levels of biotinylated total NCC and pT58-  
271 NCC being significantly greater following incubation in low chloride solution (**Fig 5A-C**).  
272 Correspondingly,  $^{22}\text{Na}$  uptakes were significantly higher in MDCKI-hNCC cells pre-

273 incubated in CF medium relative to chloride-containing (CC) medium (**Fig 5D**), indicating  
274 that in these cells a combination of increased NCC membrane expression and NCC  
275 phosphorylation correlates with greater  $^{22}\text{Na}$  uptakes.

276

277 *Acute changes in extracellular  $\text{K}^+$  concentration modulates pT58-NCC levels in MDCKI-*  
278 *hNCC cells.*

279 The activity of NCC can be directly modulated by extracellular  $[\text{K}^+]$  (39), a process that is  
280 dependent on alterations in membrane voltage and activity of the potassium channel Kir4.1  
281 (3). To assess if similar changes in NCC were evident in our system, MDCKI-hNCC cells  
282 were incubated for 15 min in buffers with different  $[\text{K}^+]$  (as KCl) and pT58-NCC levels  
283 assessed by immunoblotting (**Fig 6A**). pT58-NCC levels were inversely correlated with the  
284 extracellular  $[\text{K}^+]$  (**Fig 6B**). These changes occurred despite an absence of Kir4.1 in MDCKI-  
285 hNCC cells (**Fig 2**), suggesting an alternative  $\text{K}^+$  channel is involved in the response.  
286 Furthermore, low extracellular  $[\text{K}^+]$  increased pT58-NCC levels significantly more than  
287 incubation of cells in low chloride buffer, emphasizing that both  $\text{Cl}^-$ -dependent and -  
288 independent WNK-SPAK signalling pathways are modulated by extracellular  $[\text{K}^+]$  (30).

289

290 *Preventing phosphorylation of NCC decreases  $\text{Na}^+$  uptake, while phosphorylation-*  
291 *mimicking mutants of NCC are constitutively active*

292 To emphasize the advantages of our MDCKI isogenic stable cell lines for characterization  
293 of various NCC mutants, we performed uptake studies in MDCKI cell lines expressing; 1)  
294 rat NCC (rNCC); 2) “phospho-deficient” NCC mutants where Thr-53, Thr-58, and Ser-71 are  
295 converted to alanine (TTS-AAA) or; 3) “phospho-mimicking” NCC mutants where Thr-53,  
296 Thr-58, and Ser-71 are converted to aspartic acid (TTS-DDD) (33). Immunoprecipitation of

297 rNCC using a FLAG-tag antibody followed by western blotting identified rNCC as a non-  
298 glycosylated band of approximately 100 kDa, a mature glycosylated smeared band ~130  
299 kDa, and as dimeric forms above 250 kDa (**Fig 7A**). No NCC was detected in the absence  
300 of tetracycline. Following tetracycline induction, apical surface biotinylation followed by  
301 immunoprecipitation demonstrated similar NCC protein levels in the 3 different cell lines (**Fig**  
302 **7B**), which correlated with no significant differences in rNCC mRNA expression between the  
303 lines (**Fig 7C**). As observed for MDCKI-hNCC cells (**Fig 5A**), MDCKI-rNCC cells grown on  
304 plastic had significantly higher metolazone sensitive  $^{22}\text{Na}$  uptakes following pre-incubation  
305 CF relative to CC medium (**Fig 7D**). Under CF pre-incubation conditions, metolazone-  
306 sensitive  $^{22}\text{Na}$  uptakes in MDCKI-rNCC TTS-AAA cells were significantly lower than in  
307 MDCKI-rNCC cell lines, and almost undetectable when chloride was present in the pre-  
308 incubation medium. In contrast,  $^{22}\text{Na}$  uptakes in MDCKI-rNCC TTS-DDD mutants were  
309 significantly higher than MDCKI-rNCC cells and independent of the presence of chloride in  
310 the pre-incubation medium (**Fig 7D**).

311

312

313 **Discussion**

314           Although some studies have utilized mammalian cell lines to assess NCC function  
315 and activity, the systems used suffer from some disadvantages (summary in Table 1); 1)  
316 some have endogenous NCC expression and are thus unsuitable for assessing the activity  
317 of various NCC mutants (13, 19-21); 2) some cell lines used are not polarized and thus  
318 regulated delivery of NCC to the cell surface may be different from native cells (32); 3) the  
319 cells express NCC transiently and therefore suffer from differences in gene copy number  
320 and mRNA expression making comparisons between mutants difficult (5, 32, 40). Therefore,  
321 the majority of functional assessments of NCC, comprising a wealth of data, arise from the  
322 use of the *Xenopus laevis* expression system (4, 14, 28, 34, 43). Although this system  
323 possesses some excellent features that make it a good model system (reviewed in (25)),  
324 there exist a number of disadvantages that limit its usefulness in studying NCC function.  
325 These disadvantages include the potential for temperature-sensitive processes such as  
326 protein trafficking or transporter activity to be altered in the oocyte (derived from a  
327 poikilothermic animal), the possibility that polarized trafficking of NCC and accessory  
328 proteins are different, and the concern that complex signaling cascades and signaling  
329 specificities within oocytes are different from mammalian systems e.g. contradictory role of  
330 WNK kinases for modulation of NCC (reviewed in (1, 15)). Thus, the aim of the present study  
331 was to develop a single system that allowed for direct comparison between NCC or different  
332 NCC mutants in respect to their activity or polarized trafficking events and which had intact  
333 mammalian intracellular signaling networks.

334           The system developed utilizes MDCKI cells, which are highly characterized for  
335 studying polarized membrane protein trafficking (9, 16, 33). The cells have a single FRT site  
336 (33) and were modified to allow tetracycline-inducible expression of NCC or NCC mutants

337 from a single genetic locus ((33). The advantage of this approach is that the copy number,  
338 rate/degree of transcription, and the subsequent mRNA expression of each NCC form (as  
339 long as mRNA degradation is unaltered) should be similar (see Fig 7), and differences in  
340 NCC abundance can be attributed to post-transcriptional effects. Also, these MDCKI cells  
341 possess several elements of the signaling pathways that regulate NCC, e.g. the protein  
342 kinases SPAK, OSR1, and WNK1, -3, -4 (33), making them a suitable *in vitro* system for  
343 assessment of NCC regulatory events. This was emphasized in the current study (Fig 6),  
344 where the levels of phosphorylated NCC following alterations in extracellular [K<sup>+</sup>] mimicked  
345 the *in vivo* situation (30, 39). In the MDCKI cells, as we previously observed for rat NCC  
346 (33), human NCC existed as a highly glycosylated protein with the capacity to form dimers  
347 (Fig 1). This is an important attribute of the MDCKI-hNCC cells relative to other NCC  
348 expression systems where NCC exists predominantly as a high-mannose glycoprotein (19,  
349 21, 38), as NCC is functional as a homodimer and complex glycosylation is a prerequisite  
350 for the functional expression of NCC on the apical plasma membrane (4, 6, 17).

351 MDCKI-hNCC cells displayed robust thiazide-sensitive <sup>22</sup>Na uptake when cultured on  
352 semi-permeable supports or plastic (Fig 3). Despite reduced NCC expression, the thiazide-  
353 sensitive Na<sup>+</sup> uptakes in MDCKI-hNCC cells cultured on plastic were routinely higher than  
354 controls. The reasons for different NCC expression between the supports are unknown, but  
355 they may result from reduced polarization of the MDCK cells on plastic or the inability to  
356 absorb/secrete substances across the basolateral plasma membrane. Despite this, NCC  
357 was readily detected in the surface biotinylated pool of these cells (Fig 5) and uptake time  
358 frames (20 min), chloride dependency, and metolazone concentrations for maximal uptake  
359 inhibition were comparable to previous <sup>22</sup>Na uptake studies in mammalian cell models (7,  
360 21). Combined with the easier handling, potential for higher sample numbers, and the lower

361 experimental costs, culturing MDCKI-hNCC cells on plastic for assessment of NCC activity  
362 was deemed to be optimal.

363 Studies in oocytes or mammalian cells have demonstrated that NCC  
364 phosphorylation, plasma membrane abundance, and activity can be increased by  
365 intracellular chloride depletion (28, 32, 33). Here we demonstrated that, following  
366 intracellular chloride depletion, similar alterations in NCC function are detectable in MDCKI-  
367 hNCC cells grown on plastic. If necessary, we are able to measure NCC activity without  
368 prior intracellular chloride depletion (Fig 5), allowing us to examine regulated NCC activity,  
369 for example due to hormones such as vasopressin or angiotensin II, without prior maximal  
370 stimulation of the regulatory SPAK/OSR1 pathway. Using such an approach allowed us to  
371 demonstrate, for the first time in mammalian cells, that by mimicking NCC phosphorylation  
372 at Thr53, Thr58, and Ser71 (rat nomenclature, MDCKI-rNCC TTS-DDD mutant cells), NCC  
373 is constitutively active, whereas eliminating phosphorylation at these sites (TTS-AAA rNCC  
374 mutants) reduced  $^{22}\text{Na}$  uptake to baseline values. These data further support the idea that  
375 these sites in NCC are critical for NCC function (2, 32, 41).

376 In summary, our polarized MDCKI cell model allows rapid and direct assessment of  
377 the function of different NCC mutants. The cells can be utilized to examine the activity,  
378 localization, and abundance of different NCC mutants in the same system, and as such is  
379 highly complementary to other models currently being utilized.

380

### 381 ***Acknowledgements.***

382 We would like to thank Helle Høyer, Tina Drejer, Ahmed Abduljabar, and Christian Westberg  
383 for technical assistance. Ole Bækgaard Nielsen, Department of Biomedicine, Aarhus  
384 University is thanked for help with radiotracer studies. The original non-inducible MDCKI-  
385 FRT cells were kindly provided by Dr. Otto Froehlich, Emory University, USA (deceased).

386

387 **Grants.**

388 Funding for this study (to RAF) was provided by the Novo Nordisk Foundation, the Lundbeck  
389 Foundation and the Danish Medical Research Council. Further funding (to OS) was provided  
390 by the Swiss National Science Foundation Grant # 310030\_159735, the National Centre of  
391 Competence in Research “Swiss Kidney.ch”, networking support by the COST Action  
392 ADMIRE BM1301, the Novartis Foundation for medical-biological research. LLR is  
393 supported by the Danish Medical Research Council (Ref. DFF – 4092-00128).

394

395 **Disclosures**

396 No conflicts of interest, financial or otherwise, are declared by the authors.

397

398 **Author contributions**

399 LLR: performed experiments, analyzed data, and wrote first draft of manuscript. FR:  
400 performed experiments. NM: assisted in conception and design of experiments and  
401 analyzed data. OS: assisted in conception of experiments and analyzed data. RAF:  
402 performed experiments, conception and design of experiments, data analysis, edited and  
403 finalized manuscript. All authors approved the final version of manuscript.

404 **References**

- 405 1. **Bazua-Valenti S, and Gamba G.** Revisiting the NaCl cotransporter regulation by  
406 with-no-lysine kinases. *Am J Physiol Cell Physiol* 308: C779-791, 2015.
- 407 2. **Chiga M, Rai T, Yang SS, Ohta A, Takizawa T, Sasaki S, and Uchida S.** Dietary  
408 salt regulates the phosphorylation of OSR1/SPAK kinases and the sodium chloride  
409 cotransporter through aldosterone. *Kidney international* 74: 1403-1409, 2008.
- 410 3. **Cuevas CA, Su XT, Wang MX, Terker AS, Lin DH, McCormick JA, Yang CL,  
411 Ellison DH, and Wang WH.** Potassium Sensing by Renal Distal Tubules Requires  
412 Kir4.1. *Journal of the American Society of Nephrology : JASN* 2017.
- 413 4. **De Jong JC, Van Der Vliet WA, Van Den Heuvel LP, Willems PH, Knoers NV, and  
414 Bindels RJ.** Functional expression of mutations in the human NaCl cotransporter:  
415 evidence for impaired routing mechanisms in Gitelman's syndrome. *Journal of the  
416 American Society of Nephrology : JASN* 13: 1442-1448, 2002.
- 417 5. **de Jong JC, Willems PH, Goossens M, Vandewalle A, van den Heuvel LP,  
418 Knoers NV, and Bindels RJ.** Effects of chemical chaperones on partially retarded  
419 NaCl cotransporter mutants associated with Gitelman's syndrome in a mouse cortical  
420 collecting duct cell line. *Nephrology, dialysis, transplantation : official publication of  
421 the European Dialysis and Transplant Association - European Renal Association* 19:  
422 1069-1076, 2004.
- 423 6. **de Jong JC, Willems PH, Mooren FJ, van den Heuvel LP, Knoers NV, and  
424 Bindels RJ.** The structural unit of the thiazide-sensitive NaCl cotransporter is a  
425 homodimer. *The Journal of biological chemistry* 278: 24302-24307, 2003.
- 426 7. **de Jong JC, Willems PH, van den Heuvel LP, Knoers NV, and Bindels RJ.**  
427 Functional expression of the human thiazide-sensitive NaCl cotransporter in Madin-

- 428 Darby canine kidney cells. *Journal of the American Society of Nephrology* : JASN 14:  
429 2428-2435, 2003.
- 430 8. **Elalouf JM, Roinel N, and de Rouffignac C.** Effects of antidiuretic hormone on  
431 electrolyte reabsorption and secretion in distal tubules of rat kidney. *Pflugers Archiv*  
432 : *European journal of physiology* 401: 167-173, 1984.
- 433 9. **Frohlich O, Klein JD, Smith PM, Sands JM, and Gunn RB.** Urea transport in MDCK  
434 cells that are stably transfected with UT-A1. *Am J Physiol Cell Physiol* 286: C1264-  
435 1270, 2004.
- 436 10. **Gamba G.** Molecular physiology and pathophysiology of electroneutral cation-  
437 chloride cotransporters. *Physiological reviews* 85: 423-493, 2005.
- 438 11. **Gamba G.** Regulation of the renal Na<sup>+</sup>-Cl<sup>-</sup> cotransporter by phosphorylation and  
439 ubiquitylation. *American journal of physiology Renal physiology* 303: F1573-1583,  
440 2012.
- 441 12. **Gamba G, Miyanoshita A, Lombardi M, Lytton J, Lee WS, Hediger MA, and**  
442 **Hebert SC.** Molecular cloning, primary structure, and characterization of two  
443 members of the mammalian electroneutral sodium-(potassium)-chloride  
444 cotransporter family expressed in kidney. *The Journal of biological chemistry* 269:  
445 17713-17722, 1994.
- 446 13. **Gesek FA, and Friedman PA.** Sodium entry mechanisms in distal convoluted tubule  
447 cells. *The American journal of physiology* 268: F89-98, 1995.
- 448 14. **Glover M, Mercier Zuber A, Figg N, and O'Shaughnessy KM.** The activity of the  
449 thiazide-sensitive Na<sup>(+)</sup>-Cl<sup>(-)</sup> cotransporter is regulated by protein phosphatase PP4.  
450 *Canadian journal of physiology and pharmacology* 88: 986-995, 2010.

- 451 15. **Hadchouel J, Ellison DH, and Gamba G.** Regulation of Renal Electrolyte Transport  
452 by WNK and SPAK-OSR1 Kinases. *Annu Rev Physiol* 78: 367-389, 2016.
- 453 16. **Hoffert JD, Fenton RA, Moeller HB, Simons B, Tchapyjnikov D, McDill BW, Yu**  
454 **MJ, Pisitkun T, Chen F, and Knepper MA.** Vasopressin-stimulated increase in  
455 phosphorylation at Ser269 potentiates plasma membrane retention of aquaporin-2.  
456 *The Journal of biological chemistry* 283: 24617-24627, 2008.
- 457 17. **Hoover RS, Poch E, Monroy A, Vazquez N, Nishio T, Gamba G, and Hebert SC.**  
458 N-Glycosylation at two sites critically alters thiazide binding and activity of the rat  
459 thiazide-sensitive Na(+):Cl(-) cotransporter. *Journal of the American Society of*  
460 *Nephrology : JASN* 14: 271-282, 2003.
- 461 18. **Kim GH, Masilamani S, Turner R, Mitchell C, Wade JB, and Knepper MA.** The  
462 thiazide-sensitive Na-Cl cotransporter is an aldosterone-induced protein.  
463 *Proceedings of the National Academy of Sciences of the United States of America*  
464 95: 14552-14557, 1998.
- 465 19. **Ko B, Joshi LM, Cooke LL, Vazquez N, Musch MW, Hebert SC, Gamba G, and**  
466 **Hoover RS.** Phorbol ester stimulation of RasGRP1 regulates the sodium-chloride  
467 cotransporter by a PKC-independent pathway. *Proceedings of the National Academy*  
468 *of Sciences of the United States of America* 104: 20120-20125, 2007.
- 469 20. **Ko B, Kamsteeg EJ, Cooke LL, Moddes LN, Deen PM, and Hoover RS.** RasGRP1  
470 stimulation enhances ubiquitination and endocytosis of the sodium-chloride  
471 cotransporter. *American journal of physiology Renal physiology* 299: F300-309,  
472 2010.

- 473 21. **Ko B, Mistry AC, Hanson L, Mallick R, Cooke LL, Hack BK, Cunningham P, and**  
474 **Hoover RS.** A new model of the distal convoluted tubule. *American journal of*  
475 *physiology Renal physiology* 303: F700-710, 2012.
- 476 22. **Lemmink HH, Knoers NV, Karolyi L, van Dijk H, Niaudet P, Antignac C, Guay-**  
477 **Woodford LM, Goodyer PR, Carel JC, Hermes A, Seyberth HW, Monnens LA,**  
478 **and van den Heuvel LP.** Novel mutations in the thiazide-sensitive NaCl  
479 cotransporter gene in patients with Gitelman syndrome with predominant localization  
480 to the C-terminal domain. *Kidney international* 54: 720-730, 1998.
- 481 23. **Leviel F, Hubner CA, Houillier P, Morla L, El Moghrabi S, Brideau G, Hassan H,**  
482 **Parker MD, Kurth I, Kougioumtzes A, Sinning A, Pech V, Riemondy KA, Miller**  
483 **RL, Hummler E, Shull GE, Aronson PS, Doucet A, Wall SM, Chambrey R, and**  
484 **Eladari D.** The Na<sup>+</sup>-dependent chloride-bicarbonate exchanger SLC4A8 mediates  
485 an electroneutral Na<sup>+</sup> reabsorption process in the renal cortical collecting ducts of  
486 mice. *J Clin Invest* 120: 1627-1635, 2010.
- 487 24. **Mastroianni N, Bettinelli A, Bianchetti M, Colussi G, De Fusco M, Sereni F,**  
488 **Ballabio A, and Casari G.** Novel molecular variants of the Na-Cl cotransporter gene  
489 are responsible for Gitelman syndrome. *American journal of human genetics* 59:  
490 1019-1026, 1996.
- 491 25. **Moeller HB, and Fenton RA.** Can one Bad Egg' really spoil the batch? *J Physiol*  
492 588: 2283-2284, 2010.
- 493 26. **Moes AD, van der Lubbe N, Zietse R, Loffing J, and Hoorn EJ.** The sodium  
494 chloride cotransporter SLC12A3: new roles in sodium, potassium, and blood  
495 pressure regulation. *Pflugers Archiv : European journal of physiology* 466: 107-118,  
496 2014.

- 497 27. **Monkawa T, Kurihara I, Kobayashi K, Hayashi M, and Saruta T.** Novel mutations  
498 in thiazide-sensitive Na-Cl cotransporter gene of patients with Gitelman's syndrome.  
499 *Journal of the American Society of Nephrology : JASN* 11: 65-70, 2000.
- 500 28. **Pacheco-Alvarez D, Cristobal PS, Meade P, Moreno E, Vazquez N, Munoz E,**  
501 **Diaz A, Juarez ME, Gimenez I, and Gamba G.** The Na<sup>+</sup>:Cl<sup>-</sup> cotransporter is  
502 activated and phosphorylated at the amino-terminal domain upon intracellular  
503 chloride depletion. *The Journal of biological chemistry* 281: 28755-28763, 2006.
- 504 29. **Pedersen NB, Hofmeister MV, Rosenbaek LL, Nielsen J, and Fenton RA.**  
505 Vasopressin induces phosphorylation of the thiazide-sensitive sodium chloride  
506 cotransporter in the distal convoluted tubule. *Kidney international* 78: 160-169, 2010.
- 507 30. **Penton D, Czogalla J, Wengi A, Himmerkus N, Loffing-Cueni D, Carrel M,**  
508 **Rajaram RD, Staub O, Bleich M, Schweda F, and Loffing J.** Extracellular K<sup>+</sup>  
509 rapidly controls NaCl cotransporter phosphorylation in the native distal convoluted  
510 tubule by Cl<sup>-</sup>-dependent and independent mechanisms. *J Physiol* 594: 6319-6331,  
511 2016.
- 512 31. **Plotkin MD, Kaplan MR, Verlander JW, Lee WS, Brown D, Poch E, Gullans SR,**  
513 **and Hebert SC.** Localization of the thiazide sensitive Na-Cl cotransporter, rTSC1 in  
514 the rat kidney. *Kidney international* 50: 174-183, 1996.
- 515 32. **Richardson C, Rafiqi FH, Karlsson HK, Moleleki N, Vandewalle A, Campbell DG,**  
516 **Morrice NA, and Alessi DR.** Activation of the thiazide-sensitive Na<sup>+</sup>-Cl<sup>-</sup>  
517 cotransporter by the WNK-regulated kinases SPAK and OSR1. *Journal of cell*  
518 *science* 121: 675-684, 2008.
- 519 33. **Rosenbaek LL, Kortenoeven ML, Aroankins TS, and Fenton RA.** Phosphorylation  
520 Decreases Ubiquitylation of the Thiazide-sensitive Co-transporter NCC and

- 521 Subsequent Clathrin-mediated Endocytosis. *The Journal of biological chemistry*  
522 2014.
- 523 34. **San-Cristobal P, Pacheco-Alvarez D, Richardson C, Ring AM, Vazquez N, Rafiqi**  
524 **FH, Chari D, Kahle KT, Leng Q, Bobadilla NA, Hebert SC, Alessi DR, Lifton RP,**  
525 **and Gamba G.** Angiotensin II signaling increases activity of the renal Na-Cl  
526 cotransporter through a WNK4-SPAK-dependent pathway. *Proceedings of the*  
527 *National Academy of Sciences of the United States of America* 106: 4384-4389,  
528 2009.
- 529 35. **Sandberg MB, Riquier AD, Pihakaski-Maunsbach K, McDonough AA, and**  
530 **Maunsbach AB.** ANG II provokes acute trafficking of distal tubule Na<sup>+</sup>-Cl<sup>-</sup>  
531 cotransporter to apical membrane. *American journal of physiology Renal physiology*  
532 293: F662-669, 2007.
- 533 36. **Simon DB, Nelson-Williams C, Bia MJ, Ellison D, Karet FE, Molina AM, Vaara I,**  
534 **Iwata F, Cushner HM, Koolen M, Gainza FJ, Gitelman HJ, and Lifton RP.**  
535 Gitelman's variant of Bartter's syndrome, inherited hypokalaemic alkalosis, is caused  
536 by mutations in the thiazide-sensitive Na-Cl cotransporter. *Nature genetics* 12: 24-  
537 30, 1996.
- 538 37. **Sinning A, Radionov N, Trepiccione F, Lopez-Cayuqueo KI, Jayat M, Baron S,**  
539 **Corniere N, Alexander RT, Hadchouel J, Eladari D, Hubner CA, and Chambrey**  
540 **R.** Double Knockout of the Na<sup>+</sup>-Driven Cl<sup>-</sup>/HCO<sub>3</sub><sup>-</sup> Exchanger and Na<sup>+</sup>/Cl<sup>-</sup>  
541 Cotransporter Induces Hypokalemia and Volume Depletion. *Journal of the American*  
542 *Society of Nephrology : JASN* 28: 130-139, 2017.

- 543 38. **Subramanya AR, Liu J, Ellison DH, Wade JB, and Welling PA.** WNK4 diverts the  
544 thiazide-sensitive NaCl cotransporter to the lysosome and stimulates AP-3  
545 interaction. *The Journal of biological chemistry* 284: 18471-18480, 2009.
- 546 39. **Terker AS, Zhang C, McCormick JA, Lazelle RA, Zhang C, Meermeier NP, Siler**  
547 **DA, Park HJ, Fu Y, Cohen DM, Weinstein AM, Wang WH, Yang CL, and Ellison**  
548 **DH.** Potassium modulates electrolyte balance and blood pressure through effects on  
549 distal cell voltage and chloride. *Cell Metab* 21: 39-50, 2015.
- 550 40. **Valdez-Flores MA, Vargas-Poussou R, Verkaart S, Tutakhel OA, Valdez-Ortiz A,**  
551 **Blanchard A, Treard C, Hoenderop JG, Bindels RJ, and Jelen S.** Functionomics  
552 of Ncc Mutations in Gitelman Syndrome Using a Novel Mammalian Cell-Based  
553 Activity Assay. *American journal of physiology Renal physiology* ajprenal 00124  
554 02016, 2016.
- 555 41. **Vallon V, Schroth J, Lang F, Kuhl D, and Uchida S.** Expression and  
556 phosphorylation of the Na<sup>+</sup>-Cl<sup>-</sup> cotransporter NCC in vivo is regulated by dietary salt,  
557 potassium, and SGK1. *American journal of physiology Renal physiology* 297: F704-  
558 712, 2009.
- 559 42. **van der Lubbe N, Lim CH, Fenton RA, Meima ME, Jan Danser AH, Zietse R, and**  
560 **Hoorn EJ.** Angiotensin II induces phosphorylation of the thiazide-sensitive sodium  
561 chloride cotransporter independent of aldosterone. *Kidney international* 79: 66-76,  
562 2011.
- 563 43. **Wilson FH, Kahle KT, Sabath E, Lalioti MD, Rapson AK, Hoover RS, Hebert SC,**  
564 **Gamba G, and Lifton RP.** Molecular pathogenesis of inherited hypertension with  
565 hyperkalemia: the Na-Cl cotransporter is inhibited by wild-type but not mutant WNK4.

566 *Proceedings of the National Academy of Sciences of the United States of America*  
567 100: 680-684, 2003.  
568

569 **Figure legends**

570

571 **Fig 1: Characterization of an MDCKI cell line with tetracycline inducible human NCC**572 **expression. A:** The host MDCKI cell line contains a single FRT site and a zeocin resistance

573 gene integrated into its genome and expresses a tetracycline repressor (TR). Co-

574 transfection of pcDNA5/FRT/TO/TOPO-hNCC and pOG44 (encoding flp recombinase) into

575 the host cell line triggers homologous recombination at the FRT sites, resulting in cells with

576 a single copy of the NCC gene integrated into a specific site and displaying hygromycin

577 resistance. NCC expression is controlled by tetracycline induction via two TR binding sites

578 upstream of the NCC gene. Tetracycline treatment releases the 2xTR and transcription of

579 NCC occurs. **B:** NCC immunoprecipitated from MDCKI-hNCC cells grown on semi-

580 permeable supports using a rabbit FLAG-tag antibody. NCC is detected as a non-

581 glycosylated band of approximately 100 kDa, a glycosylated band around 130 kDa, and a

582 higher molecular weight protein above 250 kDa (possible glycosylated NCC dimers). **C:**583 Quantitative assessment of <sup>22</sup>Na uptake in MDCKI-hNCC cells grown on semi-permeable

584 supports. Cells were treated where indicated with tetracycline for 16-20 hours before uptake.

585 Uptake was performed in uptake medium +/- metolazone as indicated. <sup>22</sup>Na uptake was

586 increased by tetracycline induction and inhibited by metolazone. Data are means ± S.E.M.

587 (*n*=6). \*Represents significant differences compared to tetracycline induced cells without

588 metolazone inhibition. \*\*Represents significant differences compared to non-induced cells

589 without metolazone inhibition

590

591 **Fig 2: RT-PCR analysis of various other transport proteins in MDCKI-hNCC cells**592 **grown on semi-permeable supports.**

593

594 **Fig 3: Comparison of MDCKI-hNCC cells cultured on semi-permeable supports or**  
595 **plastic. A:** MDCKI-hNCC cells grown on plastic form a confluent monolayer of hexagonal  
596 shaped cells. **B:** NCC immunoprecipitated using a rabbit FLAG-tag antibody from MDCKI-  
597 hNCC cells grown on plastic. NCC is detected as a band around 100 kDa and a smear of  
598 approximately 130 kDa. **C:** Quantitative assessment of  $^{22}\text{Na}$  uptake in MDCKI-hNCC cells  
599 grown on semi-permeable supports or plastic. Cells were grown until confluency prior to  
600 treatment +/- tetracycline for 16-20 hours. Subsequently, cells were incubated in uptake  
601 medium +/- metolazone. In cells grown on either semi-permeable supports or plastic,  $^{22}\text{Na}$   
602 uptake is increased following tetracycline induction. However,  $^{22}\text{Na}$  uptake is significantly  
603 lower in cells grown on plastic compared to semi-permeable supports. Data are means  $\pm$   
604 S.E.M. ( $n=6$ ) \*Represents significant differences compared to MDCKI-hNCC cells grown on  
605 filters without metolazone inhibition. \*\*Represents significant differences compared to  
606 MDCKI-hNCC cells grown on plastic without metolazone inhibition. **D:** Immunoblots of NCC  
607 expression in MDCKI-hNCC cells grown on semi-permeable supports or plastic. 20S  
608 proteasome abundance is a loading control. **E:** Semi-quantitative assessment of NCC levels  
609 in MDCKI-hNCC cells grown on semi-permeable supports compared to plastic. NCC  
610 abundance is significantly lower in cells grown on plastic supports. Data are means  $\pm$  S.E.M.  
611 ( $n=3$ ) \*Represents significant difference compared to cells grown on filters.

612

613 **Fig 4: Characterization of  $^{22}\text{Na}$  uptakes in MDCKI-hNCC cells grown on plastic. A:**  
614 Effect of incubation time on  $^{22}\text{Na}$  uptake. Tetracycline induced cells were incubated in  
615 uptake medium +/- metolazone for 0 to 120 min. Data are means  $\pm$  S.E.M. ( $n=4$  per time  
616 point). There was time-linearity up to 40 min ( $r^2 = 0.95$ ). **B:** Effect of metolazone on  $^{22}\text{Na}$

617 uptake. Uptakes were performed with the indicated metolazone concentrations and data  
618 fitted to a non-linear curve with Graphpad Prism. Data are means  $\pm$  S.E.M. ( $n=6$ ). The  
619 calculated IC50 of metolazone was  $0.43 \times 10^{-6}$  C: Chloride dependency of  $^{22}\text{Na}$  uptake in  
620 MDCKI-hNCC cells. Tetracycline induced cells were pre-incubated in chloride free (CF)  
621 medium, before uptakes were performed +/- chloride or metolazone as indicated.  $^{22}\text{Na}$   
622 uptake in MDCKI-hNCC cells is not significantly different from baseline uptake when chloride  
623 is absent from uptake medium. Data are means  $\pm$  S.E.M. ( $n=12$ ) \*Represents significant  
624 differences compared to chloride-containing uptake medium without metolazone.

625

626 **Fig 5: Lowering chloride in the pre-incubation medium increases  $^{22}\text{Na}$  uptake and**  
627 **apical membrane abundance of total NCC and pT58-NCC in MDCKI-hNCC cells. A:**

628 Immunoblots showing effects of low chloride (LC) stimulation on total NCC abundance and  
629 apical plasma membrane NCC and pT58-NCC abundance in MDCKI-hNCC cells grown on  
630 plastic. 20S proteasome abundance in total homogenates is a loading control. B: Semi-  
631 quantitative assessment of biotinylated NCC levels under control or LC conditions. Plasma  
632 membrane NCC abundances significantly increase in MDCK-hNCC cells following LC pre-  
633 incubation. Data are means  $\pm$  S.E.M. ( $n=3$ ) \*Represents significant difference compared to  
634 control. C: Semi-quantitative assessment of biotinylated pT58-NCC levels following pre-  
635 incubation under control or LC. Plasma membrane pT58-NCC abundances are significantly  
636 increased with LC pre-incubation. Data are means  $\pm$  S.E.M. ( $n=3$ ) \*Represents significant  
637 difference compared to control. D: Quantitative assessment of the effect of chloride-free  
638 (CF) pre-incubation on  $^{22}\text{Na}$  uptake. Tetracycline induced cells were pre-incubated with CF  
639 or chloride-containing buffer for 20 min prior to incubation in uptake medium +/- metolazone.  
640  $^{22}\text{Na}$  uptake is significantly greater when MDCKI-hNCC cells are pre-incubated in CF buffer.

641 Data are means  $\pm$  S.E.M. ( $n=12$ ) \*Represents significant differences compared to CF pre-  
642 incubation without metolazone. \*\*Represents significant differences compared to chloride-  
643 containing pre-incubation without metolazone.

644

645 **Fig 6: Acute changes in extracellular K<sup>+</sup> concentration modulates pT58-NCC levels in**  
646 **MDCKI-hNCC cells. A:** Immunoblots of total NCC and pT58-NCC on total lysates from filter-  
647 grown MDCKI-hNCC cells treated for 15 min in different extracellular [K<sup>+</sup>]. Low chloride  
648 buffer acts as a positive control. B: Semi-quantitative assessment of extracellular K<sup>+</sup>  
649 manipulation. Data are means  $\pm$  S.E.M. ( $n=9$ ) \*Represents significant difference compared  
650 to 3 mM conditions.

651

652 **Fig 7: Role of phosphorylation at Thr53, Thr58, and Ser71 in rNCC in MDCKI-rNCC**  
653 **cells. A:** NCC immunoprecipitated from MDCKI-rNCC cells using a rabbit FLAG-tag  
654 antibody. NCC is detected as a non-glycosylated band of approximately 100 kDa, a  
655 glycosylated band around 130 kDa and a higher molecular weight protein above 250 kDa  
656 (possible glycosylated NCC dimers). **B:** Representative immunoblots of MDCKI-rNCC cells  
657 or MDCKI cells expressing phospho-deficient (TTS-AAA) or phospho-mimicking (TTS-DDD)  
658 NCC mutants. **C:** qRT-PCR to determine mRNA expression of NCC in MDCKI-rNCC, TTS-  
659 AAA, or TTS-DDD mutant cells. NCC mRNA levels are similar in the three different cell lines.  
660 **D:** Metolazone-sensitive <sup>22</sup>Na uptakes in various MDCKI-rNCC cell lines. Tetracycline  
661 induced cells were pre-incubated in chloride-free (CF) or chloride-containing (CC) medium  
662 before incubation in uptake medium +/- metolazone as indicated. Metolazone-sensitive  
663 uptake is the difference in <sup>22</sup>Na uptake between groups treated with and without metolazone.  
664 Preventing phosphorylation of NCC at Thr53, Thr58, and Ser71 inhibits <sup>22</sup>Na uptake,

665 whereas mimicking phosphorylation on the same sites renders rNCC constitutively active.

666 Data are means  $\pm$  S.E.M. ( $n=12$ ) \*Represents significant difference compared to MDCKI-

667 rNCC wt pre-incubated in CF medium.

668

**Table 1. Comparison of various systems for assessing NCC function**

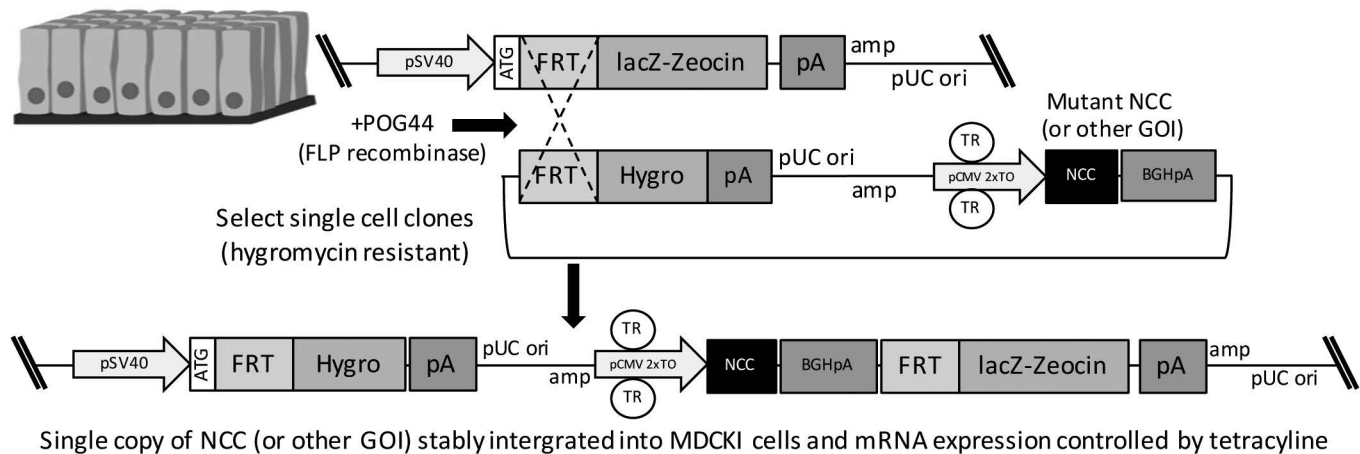
<b>System for studying NCC</b>	<b>Advantage</b>	<b>Disadvantage</b>
<b><i>Xenopus laevis</i> oocyte</b>	Easily obtained, large and hardy.	Relatively labor intensive with microinjection of each oocyte
	Few endogenous channels or transporters, resulting in low background transport	Non-native promoter and cannot be used to study NCC transcription (mRNA levels)
	Do not depend on extracellular resources for nutrition	Derived from poikilothermic animal and temperature-sensitive processes may be altered compared to mammalian cells.
	Good technical reproducibility	Accessory proteins may be different from mammalian cells
	Readily express NCC RNA that is transcribed to large amounts of exogenous protein	GPCRs and subsequent signaling cascades may be altered compared to mammalian cells
	Suitable for assessing the function of NCC mutants	Polarized NCC trafficking is not the same as mammalian cells
<b>Transiently transfected cells (HEK, CHO)</b>	Easy to transfect in high efficiency	Non-native promoter and cannot be used to study NCC transcription (mRNA levels)
	Suitable for assessing the function of NCC mutants	Not polarized and thus regulated delivery of NCC to the cell surface may be different from native cells
	Several of the GPCRs, signaling cascades and signaling specificities are comparable to native DCT cells	Suffer from differences in gene copy number and mRNA expression making comparisons between mutants difficult
<b>Endogenous NCC-expressing cells</b>	Native promoter and can be used to study NCC transcription (mRNA levels)	Unsuitable for assessing the function of NCC mutants
	Several GPCRs and subsequent signaling cascades are comparable to native DCT cells	Low NCC signal to noise
	Form polarized monolayer with apical membrane NCC expression	NCC exists predominantly as a high-mannose glycoprotein
<b>Inducible NCC expressing MDCKI cells (current study)</b>	Highly characterized mammalian cell system for studying regulated protein trafficking	Non-native promoter and cannot be used to study NCC transcription (mRNA levels)
	Form polarized monolayer with apical membrane NCC expression	Derived from dog, so commercially available reagents e.g. shRNA or antibodies against relevant NCC modulating proteins are difficult to obtain
	NCC is complex glycosylated and forms functional dimers	
	Several GPCRs and subsequent signaling cascades are comparable to native DCT cells	
	Suitable for assessing the function of NCC mutants	
	Single copy of NCC gene in cell genome making comparisons between mutants simple difficult	

672

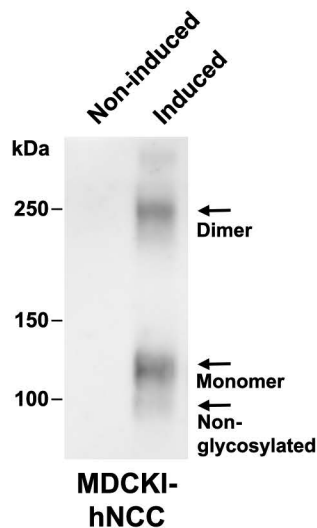
673

A

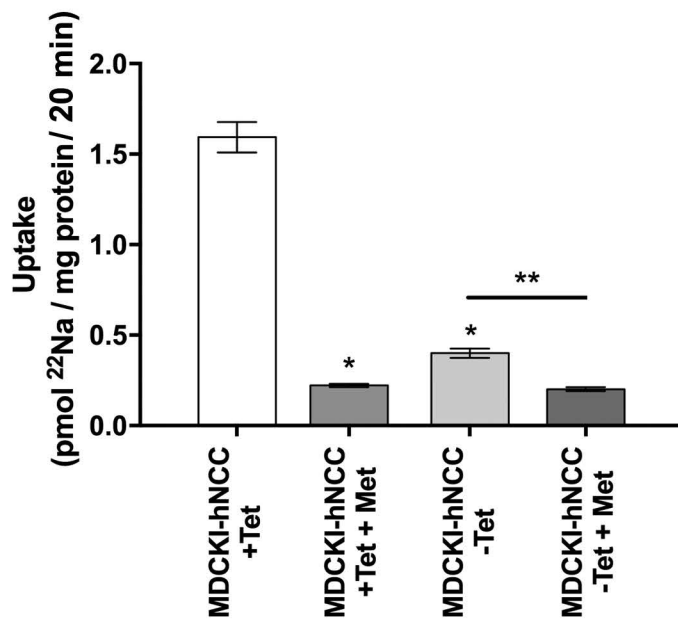
MDCKI-FRT (single integrated FRT site)

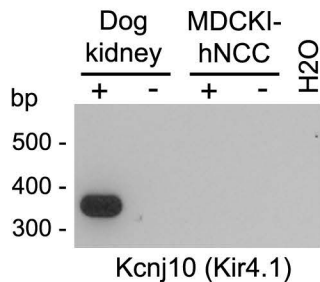
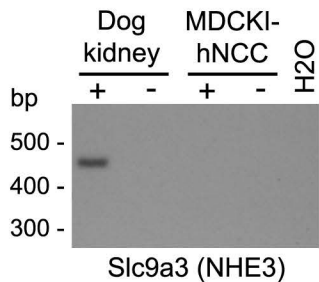
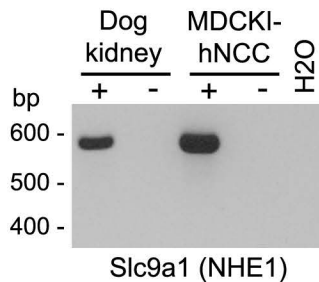
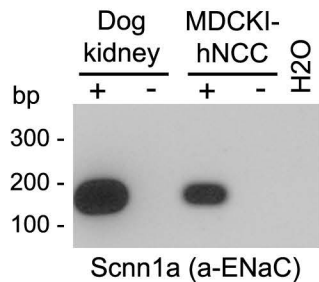
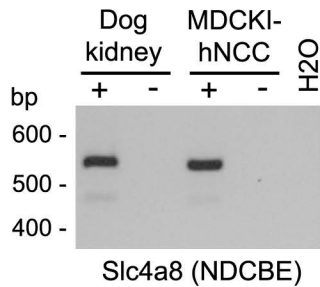
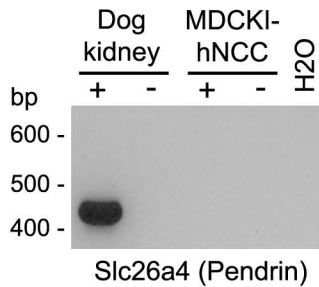
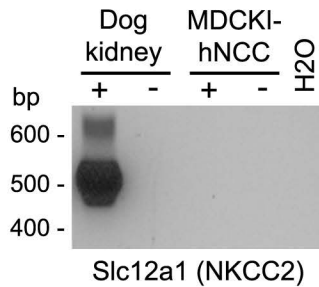
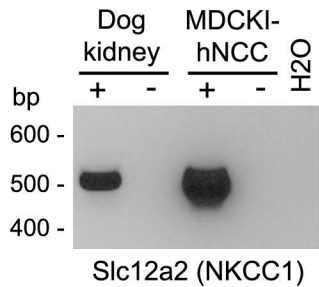


B

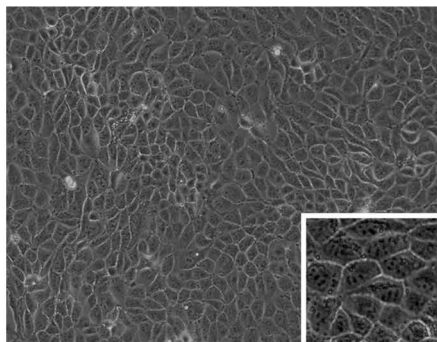


C

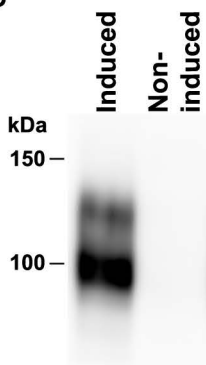




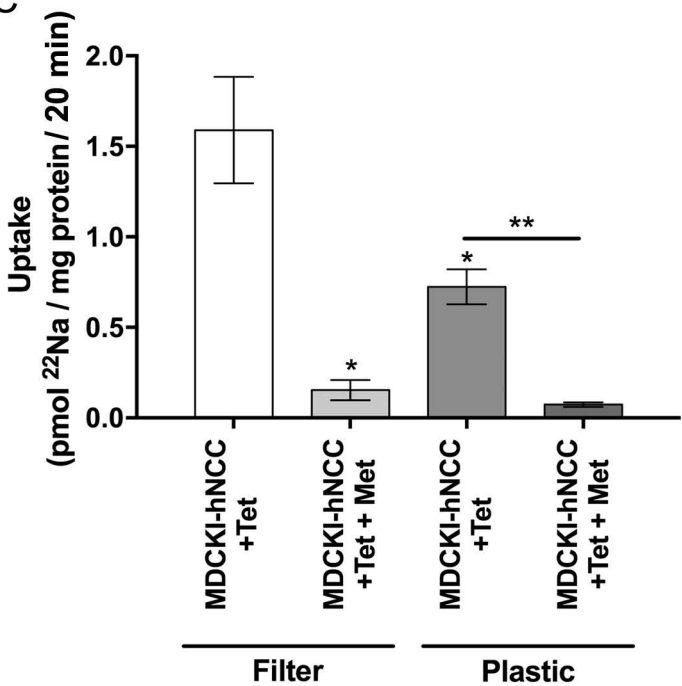
A



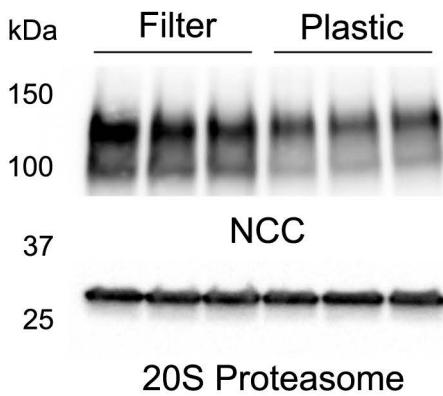
B



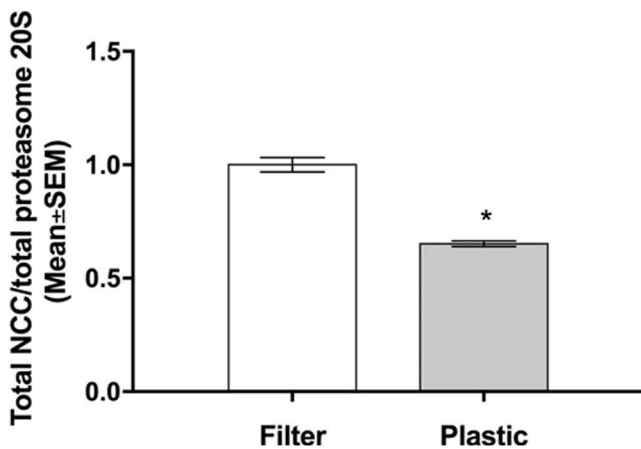
C

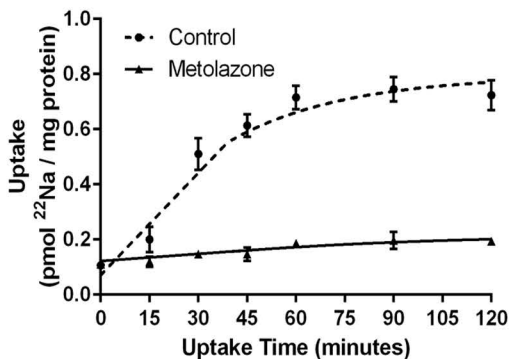
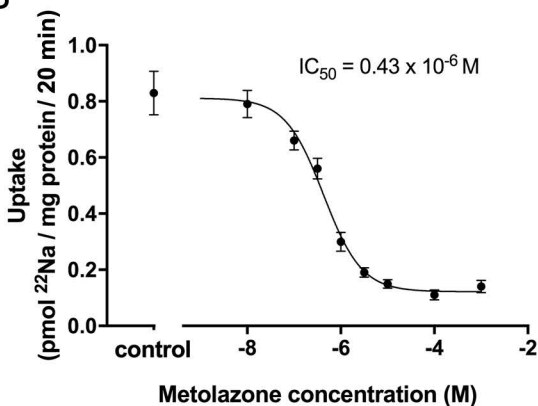
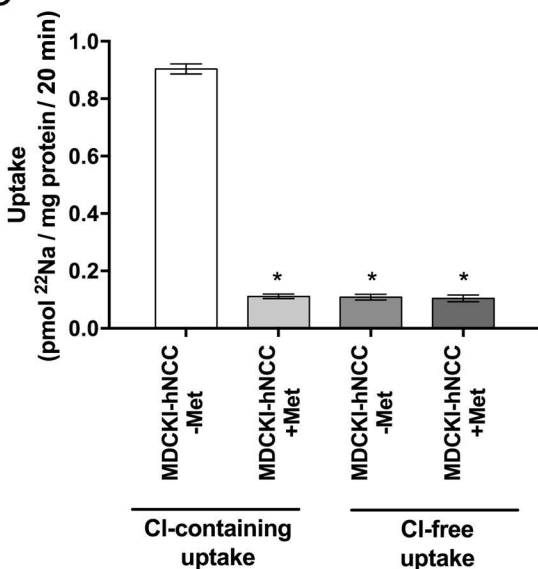


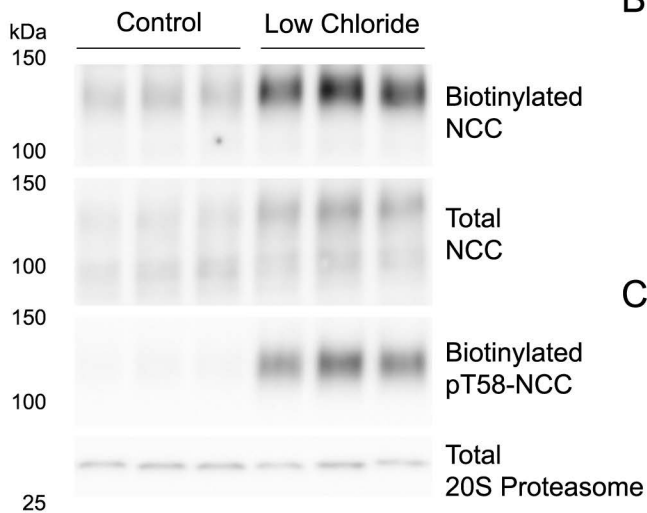
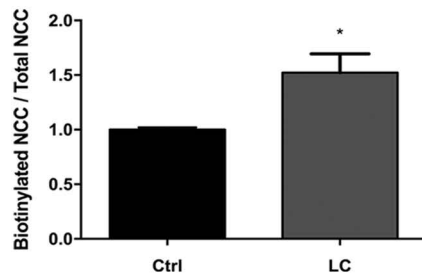
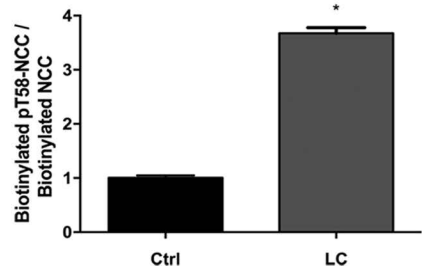
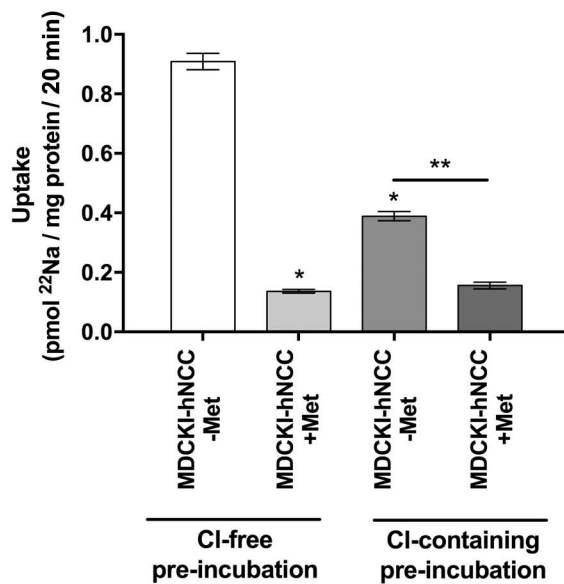
D

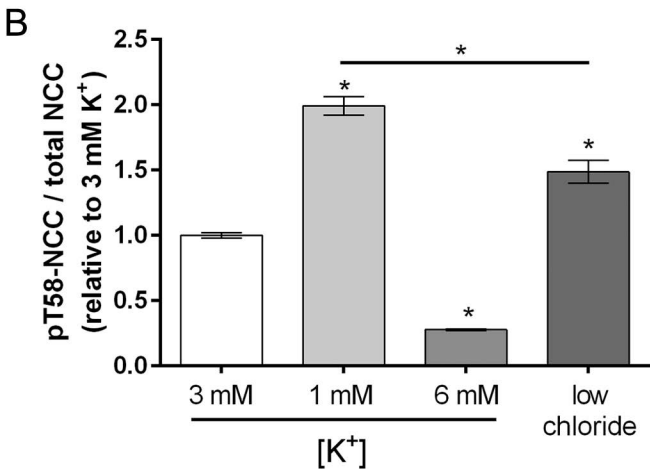
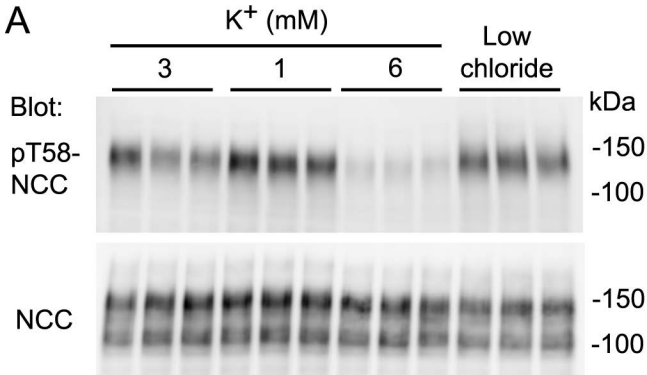


E

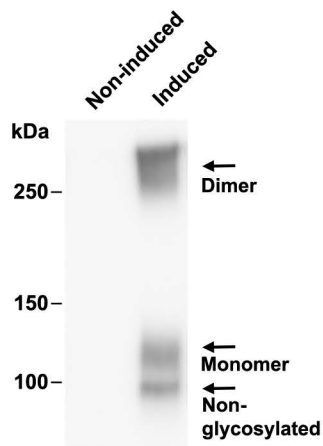


**A****B****C**

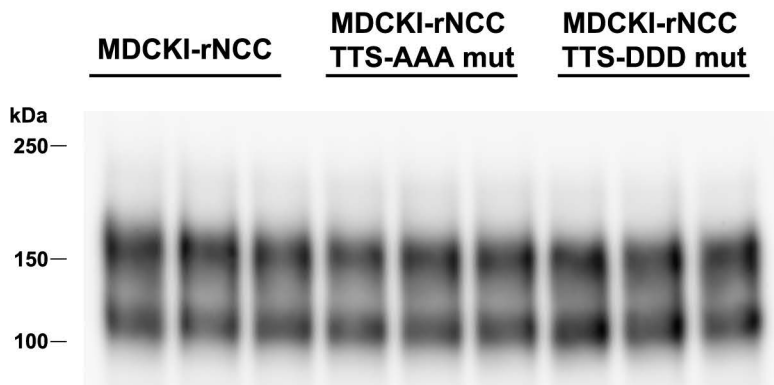
**A****B****C****D**



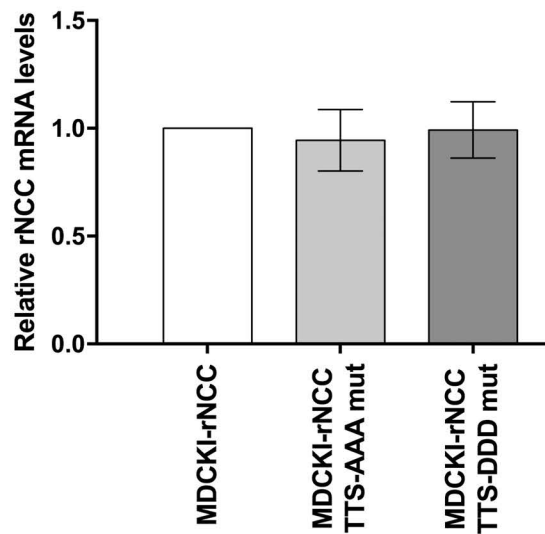
A



B



C



D

